



Seismological footprint of an anomalous atmospheric activity registered in March 2021, in Baja California, Mexico

Hortencia Flores-Estrella¹ · Lenin Ávila-Barrientos² · Hector Gonzalez-Huizar³

Received: 15 June 2022 / Accepted: 22 September 2022 / Published online: 12 October 2022
© The Author(s) 2022

Abstract

On 11 March 2021, a quite short strong signal was recorded by seismic stations of the CICESE Seismic Network, which cannot be associated with any regional or global earthquake. At the CICESE Campus and all along the city of Ensenada, in Baja California, Mexico, people reported vibration of the windows and even a short strong rumbling. Fortunately, houses and buildings did not report any damage. Due to the interaction between the atmosphere and the shallow earth surface, this anomalous atmospheric activity produced a special seismological footprint, with frequencies between 1 and 10 Hz. In this manuscript, we report on the observations of a multiparameter dataset, including seismic data along with wind velocity, wind density, temperature, humidity, atmospheric pressure, and THSW index. The atmospheric perturbation wave was strong enough to be clearly recorded by seismic stations within an area of almost 80 km and to produce some changes in the recorded meteorological parameters. The results from an FK analysis show that the atmospheric activity occurred to the south of Ensenada City and travelled to the north, as shown in the seismic records. We discuss the characteristics of the seismic signals in the frequency domain and the relation to the changes in the atmospheric parameters that could be related to this anomalous atmospheric activity.

Keywords Seismic noise · Atmospheric perturbation · FK analysis · Baja California

Introduction

In general, seismic waves are generated by earthquakes and their frequency content depends on the magnitude of the earthquake: the larger the magnitude of the earthquake, the lower the frequencies its seismic waves can reach.

Additionally, seismic signals are produced by a variety of natural and anthropogenic phenomena and sources (Fig. 1). For the frequencies of seismic interest (0.001–100 Hz), the seismological footprint of atmospheric and meteorological events, that occur near a seismological station, can be recorded and has a large influence on the ground motion (Alejandro et al. 2020; De Angelis and Bodin 2012; Gualtieri et al. 2018; Lott et al. 2017; Ritter and Groos 2007; Tanimoto and Valovcin 2016; Zürn and Meurers 2009). However, the relation between seismic signals and the characteristics of atmospheric and meteorological events is still not fully clear (Gualtieri et al. 2018; Zürn and Meurers 2009; Zürn and Widmer 1995). First, because of the complexity of the frequency-dependent energy transfer between the system atmosphere–ocean and solid earth (Gerstoft and Bromirski 2016), and because of the barometric pressure that can cause ground motion amplitudes up to $\sim 2 \mu\text{m}$, particularly over complex terrains (Holub et al. 2009) and frequencies down to $\sim 3.5 \text{ mHz}$ (Zürn et al. 2007; Zürn and Meurers 2009; Zürn and Wielandt 2007).

In general, the seismic signals generated by non-earthquake sources are called seismic noise. Several studies

Edited by Prof. Ramón Zúñiga (CO-EDITOR-IN-CHIEF).

✉ Hortencia Flores-Estrella
h.floresestrella@tu-berlin.de

- ¹ Department of Applied Geophysics, Technological University Berlin, Ernst-Reuter-Platz 1, 10587 Berlin, Germany
- ² Department of Seismology, CONACYT-CICESE, Centro de Investigación Científica Y de Educación Superior de Ensenada, Baja California (CICESE), Carretera Ensenada – Tijuana No. 3918, Zona Playitas, C. P. 22860 Ensenada, BC, Mexico
- ³ Department of Seismology, Centro de Investigación Científica Y de Educación Superior de Ensenada, Baja California (CICESE), Carretera Ensenada – Tijuana No. 3918, Zona Playitas, C. P. 22860 Ensenada, BC, Mexico

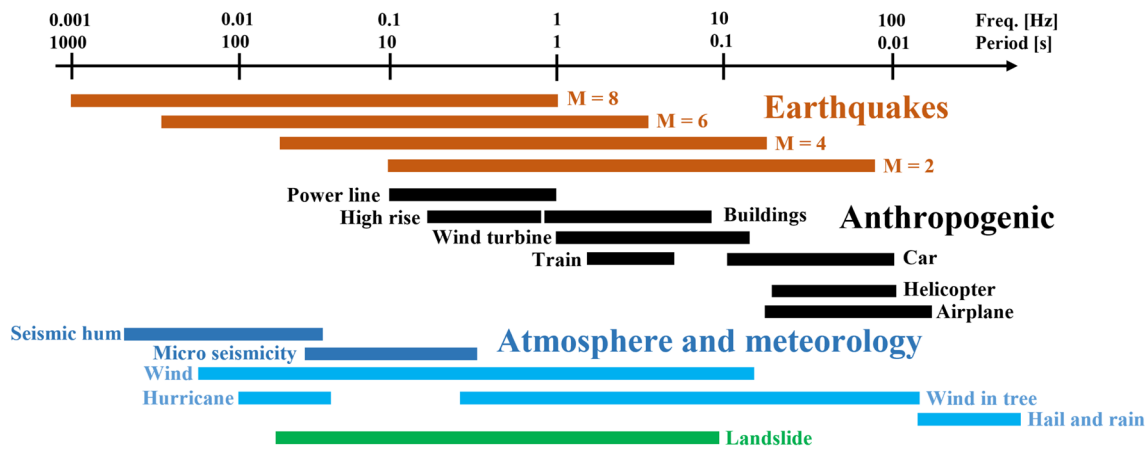


Fig. 1 Natural and anthropogenic events that originate seismic signals (after M. Weber, personal communication). In the frequencies of seismic interest (0.001 – 100 Hz), different sources are overlapped, which

makes difficult to analyse specific interesting events (Bard 1999; Bonnefoy-Claudet et al. 2006; Larose et al. 2015; McNamara and Boaz 2019)

(Alejandro et al. 2020; Ebeling and Stein 2011; Eibl et al. 2017; Gualtieri et al. 2018; Inbal et al. 2018; Lott et al. 2017; Meng et al. 2019; Meng and Ben-Zion 2018; Naderyan et al. 2016; Ritter and Groos 2007) have focussed on the identification and characterization of different sources in terms of duration, frequency content, frequency vs. time behaviour, coherency between atmospheric and seismic signals and even on the possibility to remove them from the recorded wavefield (Zürn et al. 2007; Zürn and Widmer 1995). Other studies have focussed on the location and monitoring of near-surface natural or anthropogenic seismic sources (Busert et al. 2017; De Angelis and Bodin 2012; Estrella et al. 2017; Flores et al. 2016; Friedrich et al. 2018; Gassenmeier et al. 2014; Larose et al. 2015). Moreover, the localization of "storm-quakes" as part of microseismicity (Fig. 1) has recently attracted attention (Fan et al. 2019; Gerstoft and Bromirski 2016; Guo et al. 2020).

Considering the natural non-earthquake seismic signal sources, we can see in Fig. 1 that the interaction between atmosphere–ocean and solid earth (atmosphere and meteorology in Fig. 1) plays the most important role, causing important seismic energy in the whole frequency interval of seismological interest. These sources can be separated into global sources that can be recorded no matter the location of the station (seismic hum and microseismicity) and those whose effects are more local (wind, hurricanes, hail and rain).

The so-called seismic hum appears in frequencies between 0.002 and 0.03 Hz (Bormann and Wielandt 2013; Gerstoft and Bromirski 2016; Longuet-Higgins 1950) with weak amplitudes. The source mechanisms of the seismic hum are still not completely well understood (Haned et al. 2016); however, it is assumed that the earth's hum is generated by infragravity waves and the interaction of ocean

waves with coastal waters (Bormann and Wielandt 2013; Gerstoft and Bromirski 2016).

The microseismicity can be divided into primary and secondary (Bormann and Wielandt 2013; Longuet-Higgins 1950). Primary microseismicity is characterized by a peak centred between 0.04 and 0.17 Hz (Gerstoft and Bromirski 2016), and it is generated in shallow waters and close to coastal regions due to the shoaling of ocean waves hitting the coastline (Bormann and Wielandt 2013; Gerstoft and Bromirski 2016; Holub et al. 2013). The noise excitation depends on different factors like the oceanic wave intensity, the intensity of their interferences as well as on the seafloor topography (HK Gupta 2011). Secondary microseismicity is characterized by a peak between 0.08 and 0.34 Hz and has higher spectral amplitudes than primary microseismicity (Bormann and Wielandt 2013; Gerstoft and Bromirski 2016; Holub et al. 2013). According to Borman and Wielandt (2013), it is generated by the superposition of ocean waves that have the same period but opposite travelling directions at the seafloor, responding to coupling effects of released atmospheric energy and oceanic gravity waves, which generates pressure fluctuations in the water column and that does not decay with depth (Ebeling and Stein 2011; Longuet-Higgins 1950).

The energy sources coming from meteorological events (including hurricanes, wind, rain and hail), in general, are more local, except for extreme hurricanes. In some cases, extreme meteorological events produce seismic signals with amplitudes like those of strong earthquakes at teleseismic distances (Ritter and Groos 2007) or can act as point sources with equivalent earthquake magnitudes greater than 3.5 (Fan et al. 2019). Their signal features (e.g. frequency content and amplitude) depend not only on the characteristics of the windblasts, like velocity, gusts, or direction, but also on the

pressure changes related to orography, on the topography itself, and even on local conditions like site effects (Alejandro et al. 2020; De Angelis and Bodin 2012; Gerstoft and Bromirski 2016; Gualtieri et al. 2018; Holub et al. 2009; Lott et al. 2017).

In this manuscript, we report on the observations and analysis of seismic signals caused by sudden short atmospheric signals, recorded by some stations of the CICESE seismological network, near the city of Ensenada, in Baja California, Mexico. We consider a multiparameter dataset including seismic data, atmospheric pressure, wind density, wind speed, humidity, temperature, and THSW index. We discuss the characteristics of the seismic signals in the frequency domain exploring their spectrograms, and together with meteorological data we explore possible changes in these parameters that could be due to the anomalous atmospheric activity. Finally, using FK analysis we determine its origin direction.

CICESE seismological network

The CICESE (*Centro de Investigación Científica y de Educación Superior de Ensenada, Baja California*) is the main geoscience institute in Northwestern Mexico; among other academic and scientific activities, the CICESE is responsible for the monitoring of the seismicity in Baja California, Mexico. In this region, the seismic activity is controlled by the interaction between the North American and Pacific plates which have a lateral-divergent relative motion (Fig. 2). In general, the magnitude of the most common recorded earthquakes varies from 2.0 to 5.0, with focal mechanisms that have lateral and normal components. Several earthquakes

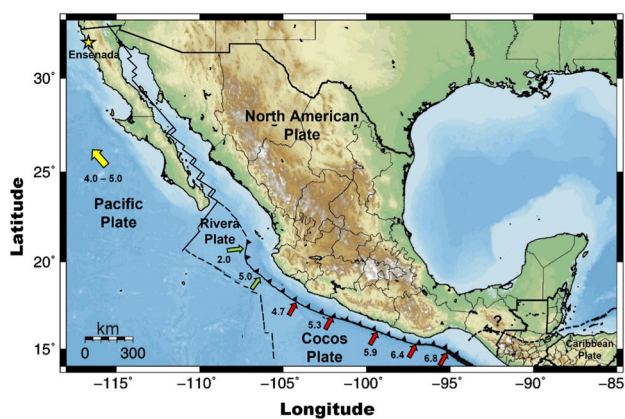


Fig. 2 Interaction of the plate tectonics located in Mexico. Arrows indicate the plate motion relative to North American plate, yellow Pacific, green Rivera, and red Cocos; and numbers indicate the plate velocity in cm/year. Yellow star marks the city of Ensenada, where the CICESE campus is located (after Ávila-Barrientos and Nava 2020)

with $M \geq 7.0$ have occurred in this region, the last one on 4 April 2010, with $M_w = 7.2$, named the Mayor-Cucapah earthquake (Castro et al. 2011). The fault system in the northern part of Baja California is composed of at least seven major faults and several smaller faults, becoming a complex system of the Pacific-North America plate boundary (Fletcher et al. 2014).

The CICESE Seismological Network (RSC, *Red Sismológica del CICESE*) main objective is to detect, record and catalogue the seismic activity that occurs in the north-western part of Mexico: northern Baja California, north-western Sonora, the southern region of the state of Baja California Sur, the Gulf of California and Nayarit. RESNOM (*Red Sísmica del Noroeste de México*) is a broad-band sub-network that belongs to the RSC and is formed by 27 stations; for this study, we consider the RESNOM broad-band stations where the seismological footprint of the atmospheric perturbation was clearly recorded (Fig. 3).

Seismological and meteorological data

On 11 March 2021, just before 20 h (UTC) a short strong signal was reported with vibration of windows and even a short strong rumbling. This phenomenon was not associated to any regional or global seismic event. We looked for a seismological footprint on the broad-band stations of RESNOM network, that we could relate to this signal to explore its spectral features and the link to atmospheric phenomena. We identified this sudden strong atmospheric signal in four broad-band stations: PBX, CCX, CBX, from RESNOM network and station TJIG from the Mexican Seismological

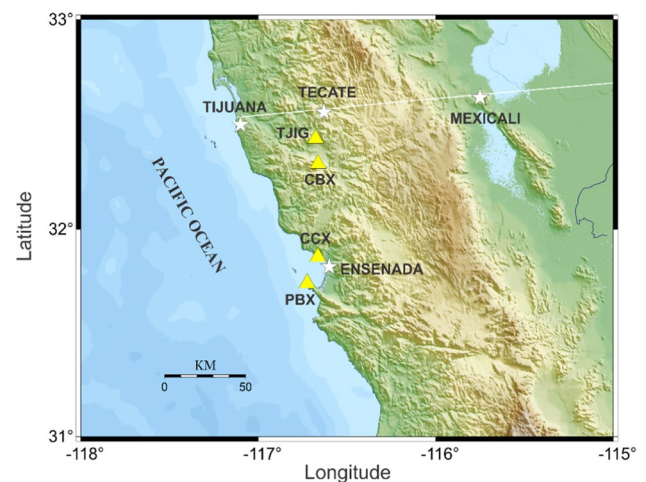


Fig. 3 Seismological stations where the seismological footprint of the atmospheric perturbation on March 11 was clearly recorded. Stations PBX, CCX, and CBX belong to the CICESE seismological network (RSC). Station TJIG belongs to the Mexican Seismological National Survey network (SSN)

Table 1 Seismological stations that recorded the seismological footprint of the atmospheric perturbation on 11 March 2021. Stations PBX, CCX, and CBX belong to the CICESE seismological network (RESNOM). Station TJIG belongs to the Mexican Seismological National Survey network (SSN)

ID	Latitude	Longitude	Elevation	Location	Network
CBX	32.3131	− 116.6630	1238	Cerro Bola	RESNOM
CCX	31.8680	− 116.6640	40	CICESE	RESNOM
PBX	31.7414	− 116.7250	351	Cerro Punta Banda	RESNOM
TJIG	32.4334	− 116.6762	317	Tijuana	SSN

National Survey network (SSN 2021) (Fig. 3 and Table 1). We also looked at the data from the CICESE meteorological station, located at the same campus as station CCX.

Seismic noise data and methodology

The stations in Table 1 record continuously with 100 samples per second all the signals produced and generated by the sources depicted in Fig. 1. After looking at all broadband stations incorporated into RESNOM, we identified the anomalous signal on the records of the four stations mentioned above (Fig. 3 and Table 1). We processed the signals by removing the instrumental response, detrend them and applied a bandpass filter between 0.1 and 25 Hz. For every motion component, we obtained spectrograms, to have a visual representation of the power variation (given in dB/Hz) of each frequency with time. We used Obspy (Beyreuther et al. 2010) for the pre-processing and to obtain the spectrograms. In Fig. 4, we show the time signals and the spectrograms of the three motion components of station CCX, located at the CICESE Campus, for 11 March 2021 between 18:30 and 21:30 h (UTC). In the time series, there is no visible change in amplitude around 20 h. However, in the spectrograms, short before 20 h a band between 1 and 10 Hz with incremented power appears in all three components.

In Fig. 5, we show the spectrograms of stations PBX, CCX, CBX and TJIG for 11 March 2021, between 18:30 and 21:30 h. The background noise level is relatively higher (frequencies with higher power) at station CCX; this can be explained because of all the urban (anthropogenic) noise near and around the station, located in the CICESE Campus. Short before 20 h, the anomalous signal is recognizable at all stations; on all the vertical components, this signal is clearly identifiable. At station PBX, it has the longest time length. At station CBX, this signal has the strongest power in comparison with all the observed stations and relatively to the background noise. In the horizontal components, the signal is visible at stations PBX, CCX and CBX but not at station TJIG. On the component NS at stations PBX and CBX, this signal is stronger as on the EW component. At station CBX,

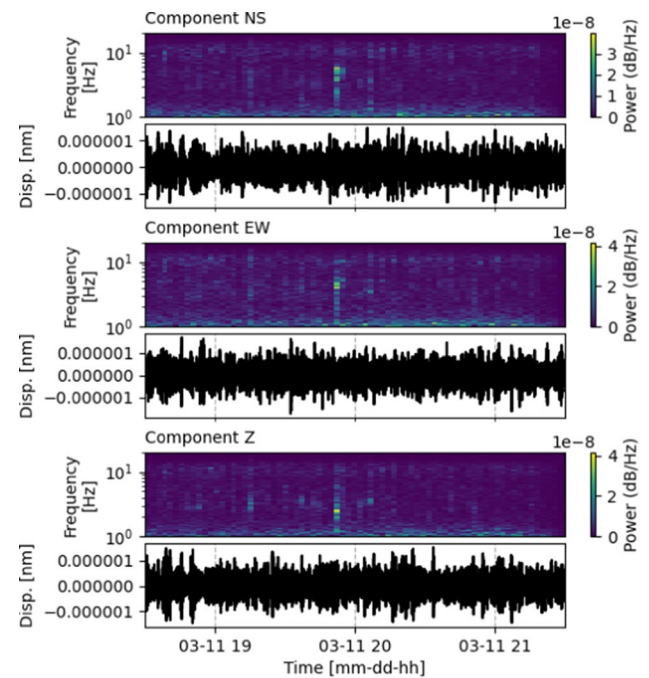


Fig. 4 Seismic signals recorded at station CCX, located at CICESE Campus, on 11 March 2021, between 18:30 and 21:30 and their spectrograms. Short before 20 h, a strong short signal is visible with a higher power in the three motion components in frequencies between 1 and 10 Hz

there is no power clear differences between components NS and EW, probably because of the higher background noise. In what follows, we consider the vertical components of the four stations.

Meteorological data

To correlate this anomalous signal with possible atmospheric disturbances, we employed the data recorded by the meteorological station located at CICESE Campus, in Ensenada. We considered the data of atmospheric pressure [mbar], the air density [kg/m^3], the wind speed [m/s], the humidity in %, the temperature [$^{\circ}\text{C}$] and the THSW index. The THSW index uses humidity, temperature, solar radiation and wind speed to calculate an apparent temperature (Table 2).

In Fig. 6, we show the variations of meteorological parameters in Table 2, between March 10 and 13. These data are measured every five minutes. Meteorological parameters usually have a 24-h periodicity (De Angelis and Bodin 2012), which is easily identifiable in the most upper panel in Fig. 6 that shows temperature and THSW index. The vertical rectangle in Fig. 6 marks the time when the anomalous short signal occurred, although any abrupt changes in the meteorological parameter are visible. However, in the bottom panel of Fig. 6 we mark with arrows some changes in

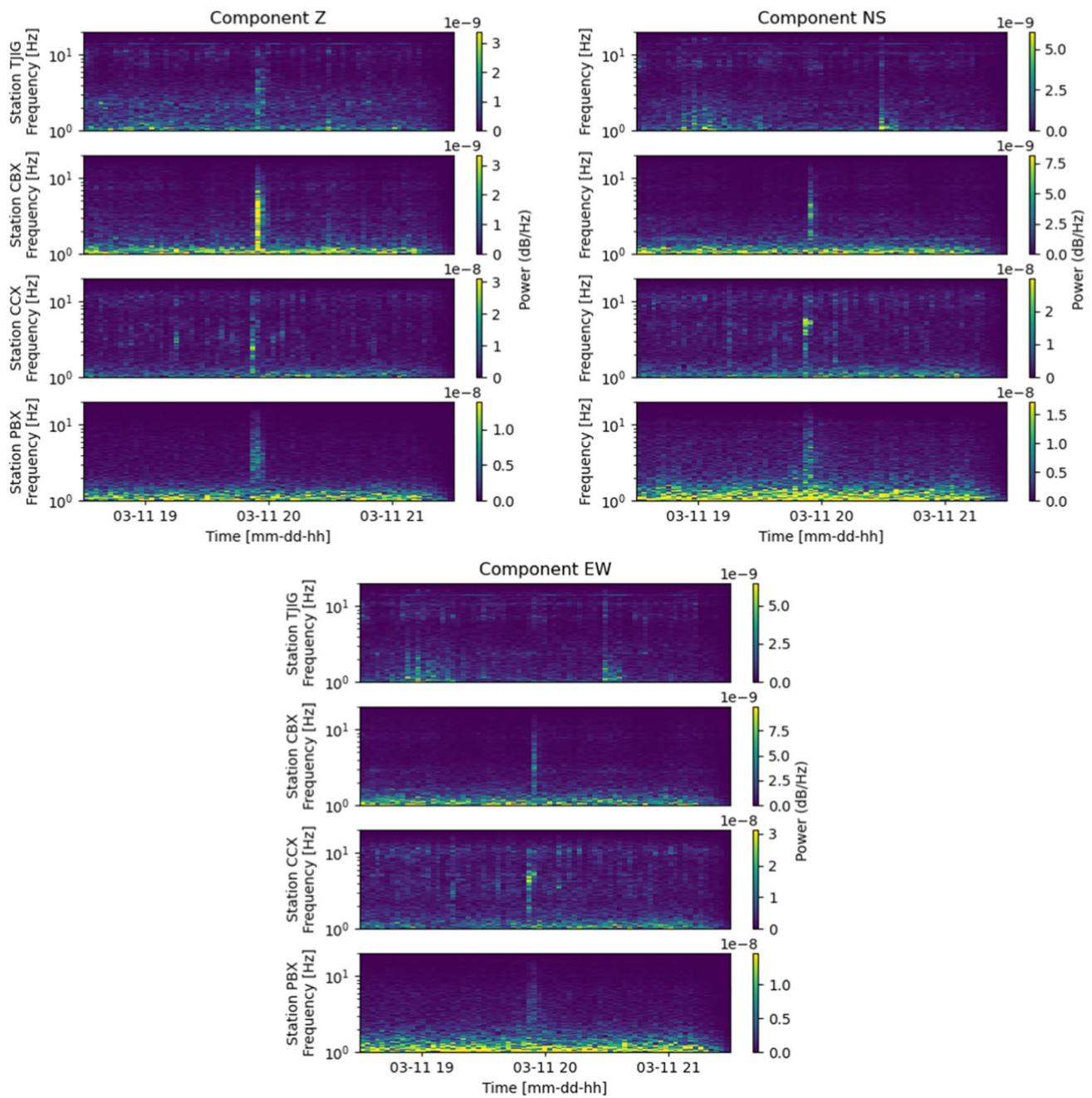


Fig. 5 Spectrograms for the three motion components of stations PBX, CCX, CBX and TJIG, on 11 March 2021, between 18:30 and 21:30 h (UTC). The anomalous signal short before 20 h is well identi-

fiable in the vertical component of all stations, not so for the horizontal components of station TJIG

Table 2 Meteorological parameters from station CCX, located at CICESE Campus, considered for our analysis

Parameter	Units
Atmospheric pressure	mbar
Wind density	kg/m ³
Wind speed	m/s
Humidity	%
Temperature	°C
THSW Index	–

the periodicity of the atmospheric pressure and the air density. For the wind density, it can be seen a 24-h periodicity with similar values for 10 and 11 March, but after the time marked with the rectangle, this value increases and keeps an increasing trend. To better understand these changes in some of the meteorological parameters and assuming a 24-h periodicity, we analyse the data for the same daytime for the three days.

Fig. 6 Meteorological parameters as measured on CICESE Campus meteorological station, between March 10 and 13. The long rectangle marks the time when the anomalous signal was recorded on the seismological stations. From this time on, an increment in the atmospheric pressure and the wind density is identifiable

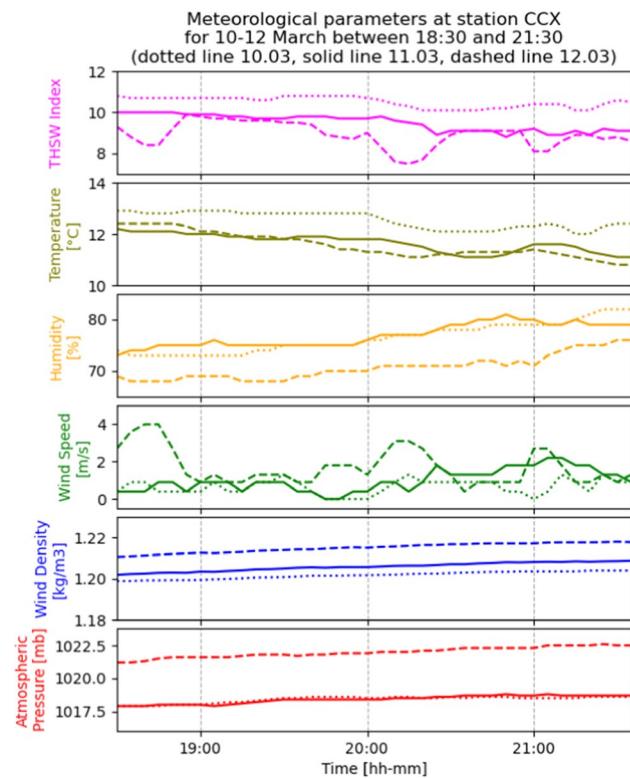
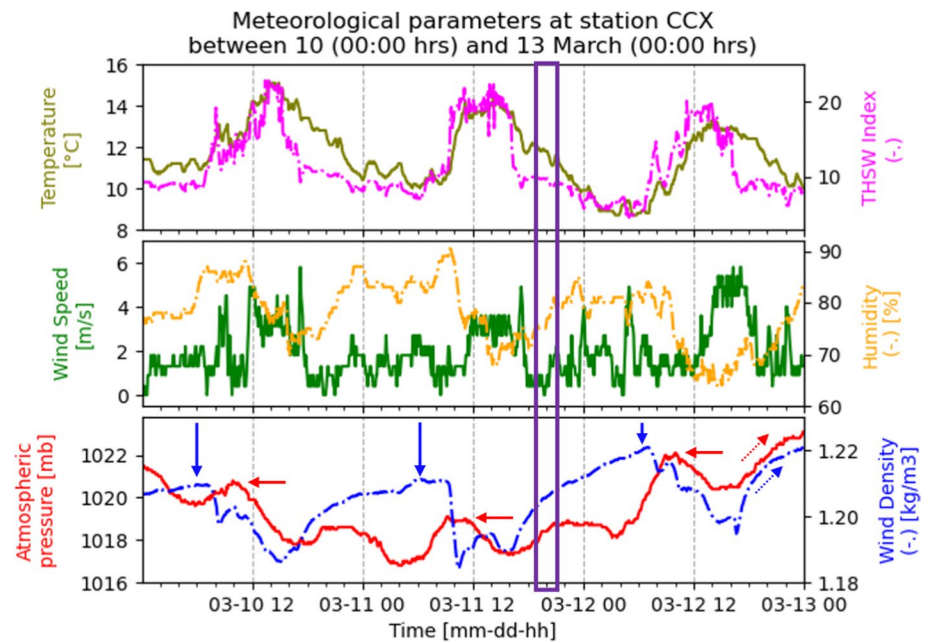


Fig. 7 Meteorological parameters as measured at the meteorological station located in CICESE campus between 18:30 and 21:30 h on three consecutive days. The major changes appear in the atmospheric pressure, wind density, wind speed, humidity, and THSW index

In Fig. 7, we show the changes on the meteorological parameters for three days, between 18:30–21:30 h; the dotted line shows the values for March 10, the solid line for

March 11 and the dashed line for March 12. In the bottom panel, for the atmospheric pressure, it is clear that for the first two days the values are almost identical, but the values for March 12 are more than 4 mbar higher. For the wind density, we have similar behaviour, the values for the third day were higher than the first two days. For March 12, the wind speed becomes more instable, especially around 20 h there are two abrupt changes, which can be associated with the variability of THSW index around the same time. The humidity diminishes for March 12, but there are no abrupt changes, and in the temperature data there are also no visible abrupt changes in the trend.

In Fig. 8, we show the spectrograms for the vertical components of the seismic noise data together with the meteorological data, for March 11, between 18:30 and 21:30 h, with a vertical rectangle we marked the seismological footprint in the spectrograms and for the meteorological parameters. The discussion of this figure is in the following section.

Discussion

The seismic noise data and the meteorological data presented in this study offer an opportunity to investigate the seismological footprint of a sudden strong atmospheric perturbation and to contribute to the knowledge about the interaction between the atmosphere and the solid earth.

The seismic noise data we use have a sampling frequency of 100 samples per second (0.01 Hz), while meteorological data are sampled every five minutes (0.003 Hz), which makes impossible a cross-correlation analysis as presented by Alejandro et al. (2020). Although it is not possible to

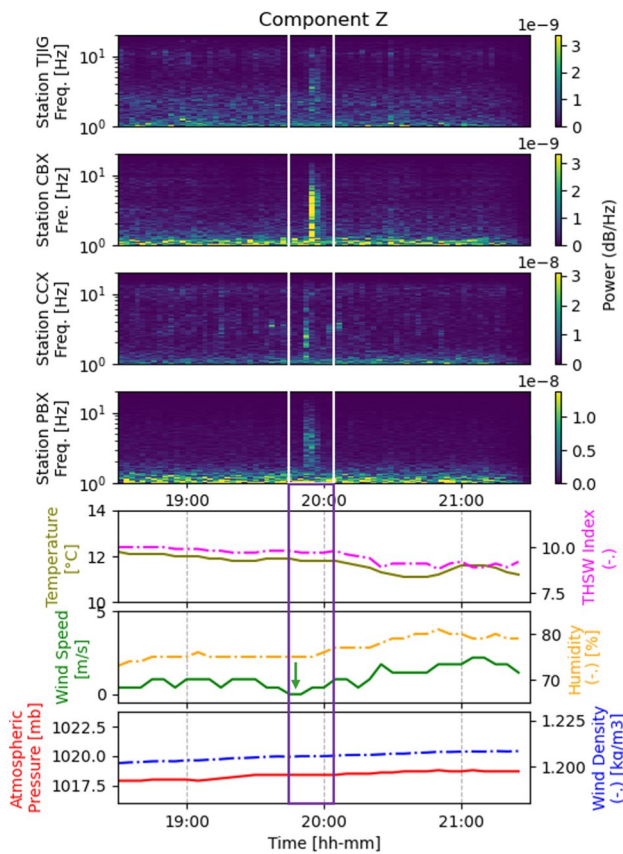


Fig. 8 Spectrograms for stations PBX, CCX, CBX and TJIG and the meteorological parameters measured at station CCX, between 18:30 and 21:30 on March 11. The vertical rectangle marks the time (short before 20:00 h) when the strong signal is visible in the spectrograms of all stations. The arrow marks a minimum in the wind speed value. More details in the text

identify a sudden change in the meteorological data, Fig. 7 shows a change in the values for March 12. Therefore, we can investigate the simultaneously variation of the seismic signal power and the meteorological data.

In Fig. 8, we show the spectrograms for the vertical components of the seismic noise data together with the meteorological data. From the spectrograms, it can be seen that the signal appears almost at the same time in PBX and CCX, but the duration is longer at PBX; a clear time delay is visible between station PBX and station TJIG, which is located almost 90 km to the NNE. Although, in this short time window when the seismic signal is well marked, there is no evidence of abrupt changes in the meteorological parameters; there are some visible particularities in the data: the temperature and the THSW index show a slight decrease; after the seismic signal, they seem to increase again. The humidity remains constant before and during perturbation and increases after it. No changes are observed in the wind density parameter, and in the atmospheric pressure, they seem to be constant before, during, and after the perturbation. The

major change is identifiable in the wind speed, it decreases to a minimum (marked with an arrow in Fig. 8), and afterwards, it increases again.

We assume this change in the wind speed is due to the atmospheric perturbation shock wave, which displaces the air around the meteorological station. This shock wave, which caused strong rumbling and windows vibration, was powerful enough to be recorded by the seismic instrumentation, even 100 km away.

A possibility to determine the features of the seismological footprint of the atmospheric perturbation, i.e. origin position and propagation velocity, is the FK analysis (Capon 1969).

FK analysis

The FK (frequency-wave number) analysis was proposed by Capon (1969) to detect nuclear explosions using the seismic network LASA (Okada 2003). Nowadays, it is one of the most commonly used techniques for the analysis of seismic noise signals recorded by arbitrary array geometries, at both small and large scales (Gal et al. 2014; Picozzi et al. 2010; Schweitzer et al. 2012; Wathelet et al. 2008), as it provides an estimation of the slowness and the directivity of seismic waves.

The FK analysis assumes that the seismic noise wavefield is formed by planewaves travelling across or along the instrumental array (Wathelet et al. 2008). For waves with a specific frequency f , the time delays between stations can be calculated to shift the phases in the frequency domain. The analysis output is given by the summation of the shifted signals and will have a maximum if the waves travel with the same direction and velocity (Capon 1969; Wathelet et al. 2008). In the wave number plane (k_x, k_y), the location of this maximum corresponds to the velocity and the azimuth of the travelling waves across the array (Wathelet et al. 2008).

In Fig. 9, we show the time signals and the spectrograms for the signals recorded on March 11, between 19:40 and 20:10 h, by the RSC stations PBX, CCX and CBX and the SSN station TJIG. In the time signals, there is no clear evidence of any particular signal. However, in the spectrograms the abrupt signals are evident in all stations, and it is clear that it arrives first to station PBX and then continues the travel to the rest of the stations. We analysed these signals with FK method for frequencies between 3 and 7 Hz, with 300 s window length, using Obspy (Beyreuther et al. 2010).

In Fig. 10, we show a polar plot with the FK results. The relative power is summed and plotted in gridded bins, that are defined by backazimuth and slowness of the analysed signal part, the backazimuth is counted clockwise from north. The colour scale corresponds to the relative power. The maximum of the beam power is located on a backazimuth $\sim 180^\circ$ and has an estimated slowness between

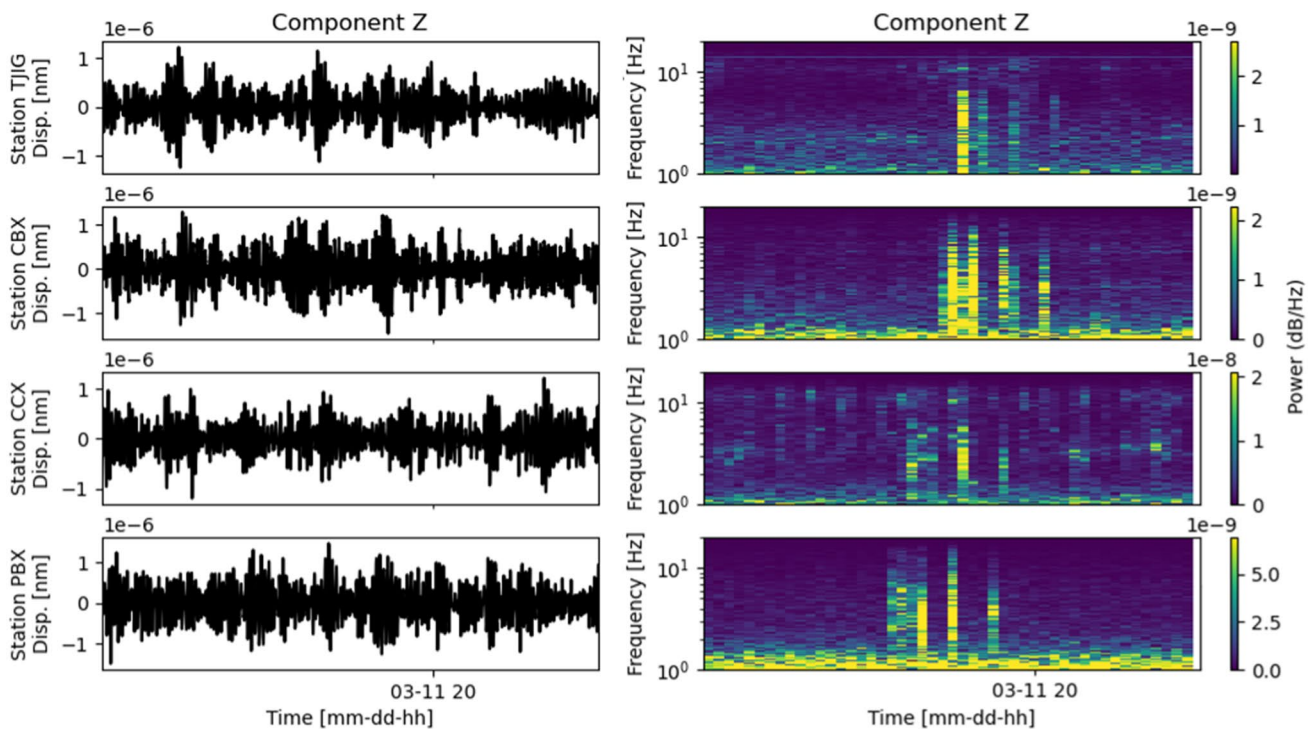


Fig. 9 Seismograms and spectrograms of the vertical component for stations PBX, CCX, CBX and TJIG between 19:40 and 20:10 on March 11. It can be seen that the signal arrives first to station PBX

and continues its travel to the other stations. We analysed these signals with FK method between 3 and 7 Hz using Obspy (Beyreuther et al. 2010)

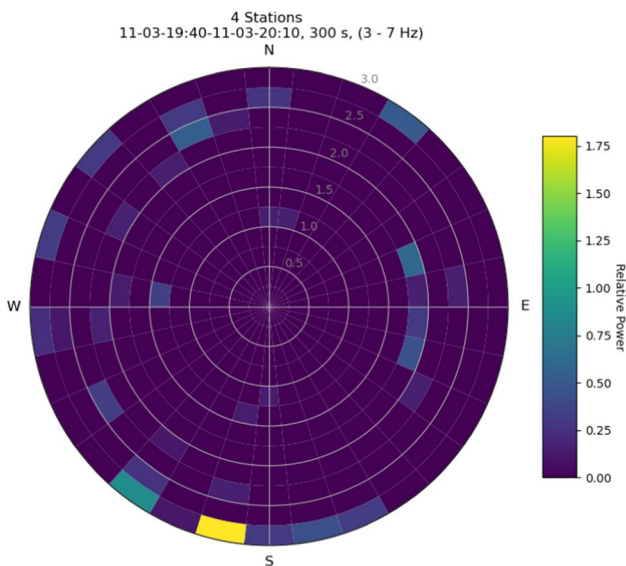


Fig. 10 Output for the FK analysis for the seismic signals in Fig. 9. The FK analysis was applied for windows with 300 s length, for frequencies between 3 and 7 Hz. The results show the maximum beam power at a backazimuth of $\sim 180^\circ$ with slowness between 2.75 and 3 s/km

2.75–3 s/km. This result confirms the observation in Fig. 9; that is, the signal comes from the south of our lineal array and travels across our stations. Furthermore, signals coming from SW have also the same slowness, but the relative power is lower than those from the south.

Conclusions

The abrupt strong atmospheric disturbance that occurred on March 11, short before 20 h, caused strong rumbling and vibrations in some windows. Though no damage or ground motion was reported, the interaction of the atmosphere with the solid earth generated seismic signals that were recorded in some stations of the RSC network and SSN. This signal is well identifiable in the vertical components of four stations, with frequencies varying between 1 and 8 Hz. In some stations, it is also visible in of the horizontal components, but probably it is masked by stronger signals.

Although the meteorological data do not show strong abrupt changes on March 11 around 20 h, a minimum in the wind speed short before the first waves arrive to PBX station, could be associated with the displacement of air around the meteorological station, due to the atmospheric perturbation shock wave.

The spectrograms of the signals show that it is recorded first on station PBX and then continues the travel to the north. This is confirmed by the results of an FK analysis for the signals between 19:40 and 20:10 h and considering frequencies between 3 and 7 Hz. We can conclude that the interaction between the strong abrupt atmospheric signal and the solid earth started south of the city of Ensenada and propagated to the north with a slowness around 2.7 and 3 s/km.

Based on our results, we can speculate that the atmospheric disturbance originated near station PBX, on Punta Banda peninsula, at the southern boundary of Todos Santos Bay. The topography of Punta Banda may have acted as a barrier, projecting the energy to the north, as we demonstrate with our analysis. We consider the role of hydrology negligible in the origin of the disturbance, because in the Punta Banda area there are only two small creeks, which could not cause a detectable signal several tens of kilometres away.

With this study, we demonstrate that the interaction of short abrupt atmospheric activity with the solid earth also generates enough energy that propagates as seismic waves that can be recorded by broad band stations as far as 100 km away.

Acknowledgements We are profoundly thankful to the RSC, SSN, and Department of Physical Oceanography (CICESE) staff for their technical support. Thanks are due to A. Mendoza Camberos, A. Pérez-Vertti, and Santiago Higareda. L. Ávila-Barrientos work at CICESE is supported by the CONACYT program Investigadoras e Investigadores por México (before Catedras CONACyT, Project 2602).

Author contributions All authors contributed to the study conception and design. The first draft of the manuscript was written by HF-E, and all authors commented on previous versions of the manuscript. All authors read and approved the final manuscript.

Funding Open Access funding enabled and organized by Projekt DEAL. No funding was obtained for this study.

Declarations

Conflict of interest The authors declare that they have no any conflict of interest.

Open Access This article is licensed under a Creative Commons Attribution 4.0 International License, which permits use, sharing, adaptation, distribution and reproduction in any medium or format, as long as you give appropriate credit to the original author(s) and the source, provide a link to the Creative Commons licence, and indicate if changes were made. The images or other third party material in this article are included in the article's Creative Commons licence, unless indicated otherwise in a credit line to the material. If material is not included in the article's Creative Commons licence and your intended use is not permitted by statutory regulation or exceeds the permitted use, you will need to obtain permission directly from the copyright holder. To view a copy of this licence, visit <http://creativecommons.org/licenses/by/4.0/>.

References

- Alejandro ACB, Ringler AT, Wilson DC, Anthony RE, Moore SV (2020) Towards understanding relationships between atmospheric pressure variations and long-period horizontal seismic data: a case study. *Geophys J Int* 223:676–691. <https://doi.org/10.1093/gji/ggaa340>
- Ávila-Barrientos L, Nava FAP (2020) Gutenberg-Richter b values studies along the Mexican subduction zone and data constraints. *Geofis Int* 59:285–298
- Bard PY (1999) Microtremor measurements: a tool for site effect estimation? The effects of surface geology on seismic motion, Irikura, Kudo. *Okada Sasatani* 3:1251–1279
- Beyreuther M, Barsch R, Krischer L, Megies T, Behr Y, Wassermann J (2010) ObsPy: a python toolbox for seismology. *Seismol Res Lett* 81:530–533. <https://doi.org/10.1785/gssrl.81.3.530>
- Bonnefoy-Claudet S, Cotton F, Bard PY (2006) The nature of noise wavefield and its applications for site effects studies. *Earth-Sci Rev* 79(3–4):205–227. <https://doi.org/10.1016/j.earscirev.2006.07.004>
- Bormann P, Wielandt E (2013) Seismic Signals and noise new manual of seismological observatory practice 2 (NMSOP2) 7 mb. Deutsc GeoForschungsZentrum GFZ. https://doi.org/10.2312/GFZ.NMSOP-2_CH4
- Bussert R, Kämpf H, Flechsig C, Hesse K, Nickschick T, Liu Q, Umlauf J, Vylita T, Wagner D, Wonik T, Flores HE, Alawi M (2017) Drilling into an active mofette: pilot-hole study of the impact of CO₂-rich mantle-derived fluids on the geo-bio interaction in the western Eger Rift (Czech Republic). *Sci Drill* 23:13–27. <https://doi.org/10.5194/sd-23-13-2017>
- Capon J (1969) High-Resolution Frequency-Wavenumber Spectrum Analysis. In: *Proceedings of the IEEE* 57
- Castro RR, Acosta JG, Wong VM, Perez-Vertti A, Mendoza A, Inzunza L (2011) Location of aftershocks of the 4 April 2010 Mw 7.2 El Mayor-Cucapah Earthquake of Baja California, Mexico. *Bull Seismol Soc Am* 101:3072–3080. <https://doi.org/10.1785/0120110112>
- De Angelis S, Bodin P (2012) Watching the wind: seismic data contamination at long periods due to atmospheric pressure-field-induced tilting. *Bull Seismol Soc Am* 102:1255–1265. <https://doi.org/10.1785/0120110186>
- Ebeling CW, Stein S (2011) Seismological identification and characterization of a large hurricane. *Bull Seismol Soc Am* 101:399–403. <https://doi.org/10.1785/0120100175>
- Eibl EPS, Lokmer I, Bean CJ, Akerlie E (2017) Helicopter location and tracking using seismometer recordings. *Geophys J Int* 209:901–908. <https://doi.org/10.1093/gji/ggx048>
- Estrella HF, Korn M, Alberts K (2017) Analysis of the influence of wind turbine noise on seismic recordings at two wind parks in Germany. *GEP* 05:76–91. <https://doi.org/10.4236/gep.2017.55006>
- Fan W, McGuire JJ, Groot-Hedlin CD, Hedlin MAH, Coats S, Fiedler JW (2019) Stormquakes. *Geophys Res Lett* 46:12909–12918. <https://doi.org/10.1029/2019GL084217>
- Fletcher JM, Teran OJ, Rockwell TK, Oskin ME, Hudnut KW, Mueller KJ, Spelz RM, Akciz SO, Masana E, Faneros G, Fielding EJ, Leprieux S, Morelan AE, Stock J, Lynch DK, Elliott AJ, Gold P, Liu-Zeng J, González-Ortega A, Hinojosa-Corona A, González-García J (2014) Assembly of a large earthquake from a complex fault system: surface rupture kinematics of the 4 April 2010 El Mayor-Cucapah (Mexico) Mw 7.2 earthquake. *Geosphere* 10:797–827. <https://doi.org/10.1130/GES00933.1>
- Flores HE, Umlauf J, Schmidt A, Korn M (2016) Locating mofettes using seismic noise records from small dense arrays and matched field processing analysis in the NW Bohemia/Vogtland Region,

- Czech Republic. *Near Surf Geophys* 14:327–335. <https://doi.org/10.3997/1873-0604.2016024>
- Friedrich T, Zieger T, Forbriger T, Ritter JRR (2018) Locating wind farms by seismic interferometry and migration. *J Seismol* 22:1469–1483. <https://doi.org/10.1007/s10950-018-9779-0>
- Gal M, Reading AM, Ellingsen SP, Koper KD, Gibbons SJ, Näsholm SP (2014) Improved implementation of the fk and Capon methods for array analysis of seismic noise. *Geophys J Int* 198:1045–1054. <https://doi.org/10.1093/gji/ggu183>
- Gassenmeier M, Sens-Schönfelder C, Delatre M, Korn M (2014) Monitoring of environmental influences on seismic velocity at the geological storage site for CO₂ in Ketzin (Germany) with ambient seismic noise. *Geophys J Int* 200:524–533. <https://doi.org/10.1093/gji/ggu413>
- Gerstoft P, Bromirski PD (2016) “Weather bomb” induced seismic signals. *Science* 353:869–870. <https://doi.org/10.1126/science.aag1616>
- Gualtieri L, Camargo SJ, Pascale S, Pons FME, Ekström G (2018) The persistent signature of tropical cyclones in ambient seismic noise. *Earth Planet Sci Lett* 484:287–294. <https://doi.org/10.1016/j.epsl.2017.12.026>
- Guo Z, Xue M, Aydin A, Ma Z (2020) Exploring source regions of single- and double-frequency microseisms recorded in eastern North American margin (ENAM) by cross-correlation. *Geophys J Int* 220:1352–1367
- Gupta HK (ed) (2011) *Encyclopedia of solid earth geophysics*. Springer, Netherlands, Dordrecht, *Encyclopedia of earth sciences series*. <https://doi.org/10.1007/978-90-481-8702-7>
- Haned A, Stutzmann E, Schimmel M, Kiselev S, Davaille A, Yelles-Chaouche A (2016) Global tomography using seismic hum. *Geophys J Int* 204:1222–1236. <https://doi.org/10.1093/gji/ggv516>
- Holub K, Rušajová J, Sandev M (2009) A comparison of the features of windstorms Kyrill and Emma based on seismological and meteorological observations. *Meteorol Zetischrift* 18:607–614. <https://doi.org/10.1127/0941-2948/2009/0409>
- Holub K, Kalenda P, Rušajová J (2013) Mutual Coupling between meteorological parameters and secondary microseisms. *Terr Atmos Ocean Sci* 24:933. [https://doi.org/10.3319/TAO.2013.07.04.01\(T\)](https://doi.org/10.3319/TAO.2013.07.04.01(T))
- Inbal A, Cristea-Platon T, Ampuero J, Hillers G, Agnew D, Hough SE (2018) Sources of long-range anthropogenic noise in Southern California and implications for tectonic tremor detection. *Bull Seismol Soc Am*. <https://doi.org/10.1785/0120180130>
- Larose E, Carrière S, Voisin C, Bottelin P, Baillet L, Guéguen P, Walter F, Jongmans D, Guillier B, Garambois S, Gimbert F, Massey C (2015) Environmental seismology: what can we learn on earth surface processes with ambient noise? *J Appl Geophys* 116:62–74. <https://doi.org/10.1016/j.jappgeo.2015.02.001>
- Longuet-Higgins MS (1950) A theory of the origin of microseisms. *Philosophical Transactions of the Royal Society of London, Mathematical and Physical Sciences*, p 38
- Lott FF, Ritter JRR, Al-Qaryouti M, Corsmeier U (2017) On the analysis of wind-induced noise in seismological recordings: approaches to present wind-induced noise as a function of wind speed and wind direction. *Pure Appl Geophys* 174:1453–1470. <https://doi.org/10.1007/s00024-017-1477-2>
- McNamara DE, Boaz R (2019) Visualization of the Seismic Ambient Noise Spectrum. In: Nakata N, Gualtieri L, Fichtner A (Eds) *Seismic Ambient Noise*. Cambridge University Press, 978–1–108–41708–2
- Meng H, Ben-Zion Y (2018) Characteristics of airplanes and helicopters recorded by a dense seismic array near Anza California. *J Geophys Res Solid Earth* 123:4783–4797. <https://doi.org/10.1029/2017JB015240>
- Meng H, Ben-Zion Y, Johnson CW (2019) Detection of random noise and anatomy of continuous seismic waveforms in dense array data near Anza California. *Geophys J Int* 219:1463–1473. <https://doi.org/10.1093/gji/ggz349>
- Naderyan V, Hickey CJ, Raspet R (2016) Wind-induced ground motion. *J Geophys Res Solid Earth* 121:917–930. <https://doi.org/10.1002/2015JB012478>
- Okada H (2003) The microtremor survey method. *Society of Exploration Geophysicists, Geophysical Monograph Series*, p 135
- Picozzi M, Parolai S, Bindi D (2010) Deblurring of frequency-wave-number images from small-scale seismic arrays. *Geophys J Int* 181:357–368. <https://doi.org/10.1111/j.1365-246X.2009.04471.x>
- Ritter JRR, Groos J (2007) Der Orkan Kyrill ließ auch den Boden erzittern. *Spektrum der Wissenschaft*, März 2007, S. 19. *Spektrum der Wissenschaft Verlagsgesellschaft mbH, Heidelberg, Deutschland*
- Schweitzer J, Fyen J, Mykkeltveit S, Gibbons SJ, Pirl M, Kühn D, Kværna T (2012) *Seismic arrays new manual of seismological observatory practice 2 (NMSOP2) 6 mb*. *Deutsch GeoForschungsZentrum GFZ*. https://doi.org/10.2312/GFZ.NMSOP-2_CH9
- SSN (2021) *Universidad Nacional Autónoma de México, Instituto de Geofísica, Servicio Sismológico Nacional, México*. <http://www.ssn.unam.mx>
- Tanimoto T, Valovcin A (2016) Existence of the threshold pressure for seismic excitation by atmospheric disturbances: critical pressure for seismic excitation. *Geophys Res Lett* 43:11202–11208. <https://doi.org/10.1002/2016GL070858>
- Wathelet M, Jongmans D, Ohrnberger M, Bonnefoy-Claudet S (2008) Array performances for ambient vibrations on a shallow structure and consequences over V s inversion. *J Seismol* 12:1–19. <https://doi.org/10.1007/s10950-007-9067-x>
- Zürn W, Meurers B (2009) Clear evidence for the sign-reversal of the pressure admittance to gravity near 3mHz. *J Geodyn* 48:371–377. <https://doi.org/10.1016/j.jog.2009.09.040>
- Zürn W, Widmer R (1995) On noise reduction in vertical seismic records below 2 mHz using local barometric pressure. *Geophys Res Lett* 22:3537–3540. <https://doi.org/10.1029/95GL03369>
- Zürn W, Wielandt E (2007) On the minimum of vertical seismic noise near 3 mHz. *Geophys J Int* 168:647–658. <https://doi.org/10.1111/j.1365-246X.2006.03189.x>
- Zürn W, Exß J, Steffen H, Kroner C, Jahr T, Westerhaus M (2007) On reduction of long-period horizontal seismic noise using local barometric pressure. *Geophys J Int* 171:780–796. <https://doi.org/10.1111/j.1365-246X.2007.03553.x>